Data Assimilation of Satellite-Derived Arctic Sea-Ice Thickness During Boreal Summer

Jeong-Gil Lee, Daehyun Kang, Joo-Hong Kim, Jong-Min Kim, Sang-Moo Lee, *Member, IEEE*, and Yoo-Geun Ham

***Abstract*—Reliable estimation and initialization of Arctic sea-ice thickness (SIT) through data assimilation (DA) during the summer melt season were previously hampered by the lack of available observations owing to limitations in satellite retrieval algorithms. Recently, successful satellite-derived Arctic SIT measurements from CryoSat-2 (CS2) and advanced microwave scanning radiometer 2 (AMSR2) during the boreal summer have been achieved using advanced retrieval algorithms. This study compares the impacts of CS2 and AMSR2 SIT datasets by individually assimilating each dataset using the ensemble optimal interpolation DA technique with CICE 5 dynamical sea-ice model in 2019 and 2020. The underestimated sea-ice extent in the control simulation without DA during summer was effectively corrected in the reanalysis assimilating AMSR2. However, the degree of correction was less pronounced in the reanalysis assimilating CS2. A sensitivity experiment confirmed that the weak correction degree when using CS2 was not due to its low spatiotemporal resolution, suggesting that the issues may arise from a systematic negative bias related to ice roughness over the central Arctic Ocean in CS2. During the summer and subsequent sea-ice growing seasons, the simulated SIT in the DA of AMSR2 shows greater similarity with independent reanalysis and satellite data than that of CS2. Validations against SIT observations measured by ice mass balance and upward-looking sonar indicate that the DA of AMSR2 effectively enhances the day-to-day variability compared with CS2 and control simulations during both the summer and subsequent winter seasons. This study underscores the response of the model to assimilating current satellite summer SIT data and highlights the factors to consider when utilizing these data.**

Received 11 February 2025; revised 23 March 2025; accepted 9 April 2025. Date of publication 16 April 2025; date of current version 5 May 2025. This work was supported in part by Korea Polar Research Institute (KOPRI) grant funded by the Ministry of Oceans and Fisheries under Grant KOPRI PE25010 and in part by Korea Meteorological Administration Research and Development Program under Grant RS-2024-00403698. *(Corresponding authors: Sang-Moo Lee; Yoo-Geun Ham.)*

Jeong-Gil Lee is with the Environmental Planning Institute, Seoul National University, Seoul 08826, South Korea (e-mail: jeonggil@snu.ac.kr).

Daehyun Kang is with the Center for Climate and Carbon Cycle Research, Korea Institute of Science and Technology, Seoul 02792, South Korea (e-mail: dkang@kist.re.kr).

Joo-Hong Kim is with the Division of Ocean and Atmosphere Sciences, Korea Polar Research Institute, Incheon 21990, South Korea (e-mail: joo-hong.kim@kopri.re.kr).

Jong-Min Kim is with the Center of Remote Sensing and GIS, Korea Polar Research Institute, Incheon 21990, South Korea (e-mail: jmkim@kopri.re.kr).

Sang-Moo Lee is with the School of Earth and Environmental Sciences and the Institute for Data Innovation in Science, Seoul National University, Seoul 08826, South Korea (e-mail: sangmoolee@snu.ac.kr).

Yoo-Geun Ham is with the Department of Environmental Managements, Graduate School of Environmental Studies, Seoul National University, Seoul 08826, South Korea, and also with Environmental Planning Institute, Seoul National University, Seoul 08826, South Korea (e-mail: yoogeun@snu.ac.kr).

This article has supplementary downloadable material available at https://doi.org/10.1109/JSTARS.2025.3561257, provided by the authors.

Digital Object Identifier 10.1109/JSTARS.2025.3561257

***Index Terms*—Advanced microwave scanning radiometer 2 (AMSR2), CryoSat-2 (CS2), data assimilation (DA), sea-ice thickness (SIT), summer sea ice.**

I. Introduction

Arctic sea ice has been undergoing rapid and significant changes due to anthropogenic climate change, as evidenced by the dramatic decline in summer sea-ice extent (SIE) (defined as the cumulative area of all grid cells with sea-ice concentration (SIC) greater than 0.15) and sea-ice thickness (SIT) [1], [2]. As a critical component of the Earth's cryosphere, summer sea ice is vital for regulating both regional and global climate systems [3], influencing atmospheric and oceanic circulation patterns over the Northern Hemisphere [4], [5] and affecting ecosystems and human activities [6] in the Arctic. Consequently, the accurate modeling and prediction of the summer sea-ice amount are essential for understanding these transformations and their broader implications.

To precisely predict sea-ice amounts using dynamical models, data assimilation (DA) techniques have been implemented to secure realistic initial conditions by incorporating satellite-derived sea-ice observations [7], [8], [9]. SIT, a critical prognostic variable of sea-ice models, shows significant spatial autocorrelation and is the most reliable predictor, second only to sea-ice volume itself [10]. SIT anomalies, which exhibit longer persistence than SIE anomalies [11], provide predictive insights into SIE anomalies [12], [13]. Thus, the positive impacts of SIT DA on the simulations are widely recognized for both SIE and SIT [14], [15], [16].

Until recently, most DA studies incorporating satellite SIT primarily focused on the boreal winter season because of the lack of a reliable retrieval technique for remotely sensed SIT during other seasons, such as the melting season from late May to September. Observing SIT during boreal summer is complicated by the heterogeneous surface characteristics of melted sea ice, which pose challenges to the conventional algorithms designed for winter conditions [17], [18], [19], [20]. For instance, Tilling et al. [19] noted the difficulty in distinguishing measurements from open water and sea ice from May to September.

In addition to the challenges in initialization due to the absence of accurate observations, the prediction skill of Arctic sea ice during the melt season is constrained by a spring predictability barrier [21], [22], [23], [24], [25]. Specifically, predictions initialized before spring, particularly in May, exhibit much lower

accuracy than those initiated on or after this date in both statistical [26], [27], [28], [29] and dynamical models [12], [30]. Previous research has demonstrated that the preconditioning of early summer SIT anomalies is crucial for accurately predicting sea ice in September [27], [31], [32], [33], underscoring the significance of SIT observations gathered during the melt season (May–August) for seasonal predictions of Arctic summer sea ice at a regional level.

Recent developments in sophisticated algorithms have enhanced the estimation of summer SIT, facilitating the retrieval of summer SIT or related variables, such as the sea-ice draft (i.e., underwater depth of sea ice below sea level; SID) [34], [35] from satellite measurements. One source of satellite-based summer SIT data was derived from synthetic aperture interferometric radar altimeter/CryoSat-2 observations [34], a part of the year-round Arctic SIT observations during 2011–2022 using CryoSat-2 radar freeboard correction under summer ice conditions. Another source is retrieved from the advanced microwave scanning radiometer (AMSR) 2 [35] onboard the global change observation mission for water (GCOM-W). These data are based on a method for estimating SID based on spaceborne passive microwave-measured brightness temperatures.

The quality of satellite-derived SIT has been extensively assessed using independent in situ observations with higher accuracy. In particular, Beaufort Gyre Exploration Project (BGEP) mooring data from Woods Hole Oceanographic Institution and Seasonal Ice Mass Balance Buoy 3 (SIMB3) buoy data from cryosphere innovation have been widely utilized for the validation of satellite-retrieved products [19], [36], [37], [38], [39].

When validated against in situ observations, AMSR2 SIT produces more accurate satellite estimates compared with CryoSat-2. CryoSat-2 SID, when compared with BGEP SID measurements from June to August during 2013–2018, was found to be underestimated [34]. In contrast, AMSR2-based SID estimates demonstrated better agreement with the in situ observations [35]. For intercomparison, after rescaling AMSR2 SID to match the spatiotemporal resolution of CryoSat-2, the root-mean-square error (RMSE) was 0.48 m with a bias of −0.19 m. Meanwhile, CryoSat-2 SID exhibited a higher RMSE of 0.85 m and a bias of −0.56 m [35].

Recent advancements in summer SIT observations from satellites enable more reliable SIT reanalysis fields of SIT through the DA of these SIT data into dynamical models, offering promising prospects for improving Arctic sea-ice predictions during the melting season. For instance, several studies have explored the positive impacts of the DA of year-round CryoSat-2 SIT during summer on seasonal predictions of sea-ice conditions [40], [41], [42]. Song et al. [42] found that initializing SIT using daily interpolated and spatially upsampled fields from biweekly CryoSat-2 SIT data along with adjustments for observational uncertainties in thick ice regions during the ice-melting season of 2015/16 led to improved predictions of summer ice-edge forecast errors. Zhang et al. [41] demonstrated that assimilating spatiotemporally upsampled CryoSat-2 SIT daily anomalies with a 1° horizontal resolution from May to August enhanced the accuracy of local September SIC and SIE predictions from 2011 to 2020. Min et al. [40] also showed that the daily updates of the SIT initial conditions through incremental analysis updates for the CryoSat-2 summer SIT from May to September 2016 improved the overestimation in the reanalysis produced by the combined model and satellite thickness [43]. In contrast, while the impact of SIT from CryoSat-2 has been extensively studied through assimilation, the effects of AMSR2-estimated SIT data have not yet been explored. As the two datasets utilize distinct sensors and retrieval algorithms, providing different SIT estimates and resolutions in space and time, the influence of each data on the model via DA may vary.

In this study, the impact of the satellite-derived SIT observations obtained from CryoSat-2 and AMSR2/GCOM-W during the melting period was investigated by assimilating them into the Community Ice CodE version 5.1.2 (CICE5) through the ensemble optimal interpolation (EnOI) scheme [44], [45], [46]. The reanalyzed sea-ice fields were assessed for both summer and subsequent winter seasons using independent reanalysis and in situ observations. The rest of this article is organized as follows. Section II describes the models and methods used. Section III evaluates the impact of DA on sea-ice conditions. Finally, Section IV concludes this article.

II. Methods

A. Model and Boundary Conditions

This study used the CICE5 sea-ice dynamical model developed by the Los Alamos National Laboratory [47]. The CICE5 model is a state-of-the-art sea-ice prediction model with complex physical parameterization schemes and serves as the sea-ice component of the National Center for Atmospheric Research Community Earth System Model [48]. The CICE5 model classifies the ice thickness distribution into five categories with each category comprising seven vertical ice layers and one snow layer to account for variations in sea-ice temperature and salinity. The model uses mushy layer thermodynamics for handling thermodynamic processes and elastic-anisotropic–plastic dynamics for dynamic processes [49], [50]. In addition, it incorporates recent complex physics parameterization schemes, including those for melt ponds and pressure ridging [51], [52]. The model covers all longitudes and latitudes poleward to 89.71°N, operates at a horizontal resolution of approximately 1° on a displaced pole grid with dimensions of 320 × 384, and employs a time step of 1 h.

The atmospheric boundary forcings for CICE5, including surface momentum (i.e., zonal and meridional wind stresses) and surface heat fluxes (i.e., incoming and outgoing longwave and shortwave radiations), are based on the National Centers for Environmental Prediction-Department of Energy Reanalysis 2 dataset [53]. In addition, the modeled sea surface temperature (SST) data are nudged toward the optimal interpolation SST version 2 from the National Oceanic and Atmospheric Administration [54] with a restoring timescale of 20 days.

B. DA Scheme

The satellite-derived SIT observations were assimilated into the CICE5 model using an EnOI scheme with a 1-day assimilation cycle [46], [55], [56], [57]. The EnOI scheme

employs a stationary ensemble member to approximate the background error covariance matrix. This offers a cost-effective alternative to the ensemble Kalman filter, especially in situations with limited computational resources [58]. The stationary ensemble members or background error perturbations for the EnOI were generated using a methodology similar to that used to obtain bred vectors [59]. To capture seasonal variations in the spatial distribution of the perturbations, the background error covariance matrix for any given day was computed using the background perturbations from the corresponding day across the years 1982–2019. Consequently, the background error covariance matrix exhibits a seasonal cycle, with 38 samples contributing to its formulation on any given day (i.e., one sample per year). For further details on the equations and schematics, refer to the previous study [44]. It is noted that changes from SIT DA are applied only to grid cells where the SIC exceeds a conservatively set threshold of 0.15 [14], [15], [16]. This means that SIT DA does not create additional sea ice in empty grid cells (i.e., open water).

C. CryoSat-2 and AMSR2 Data for DA

In this study, we used the year-round pan-Arctic CryoSat-2 SIT and the corresponding observation error dataset for DA during the summer season [34], which we refer to herein as CS2. Landy et al. [34] applied melting correction to the ice freeboard during the melt season. The corrected ice freeboard was then converted to SIT using the hydrostatic assumption along with model-based snow depth and snow density values. The observational error averaged during the ice-melting season of CS2 is 0.41 m [41]. For this study, biweekly CS2 summer SIT data with 80-km spatial resolution covering the period from June to August 2019 and from June to July 2020 were obtained from the British Antarctic Survey webpage.

For the DA, we also utilized AMSR2-based SID dataset [35]. This dataset is estimated through a method for the pan-Arctic SID during the melt season by empirically relating AMSR2 brightness temperatures to the BGEP upward-looking sonar (ULS) measured SID. The spatial resolution of the SID estimation is 25 km, with daily temporal resolution covering the periods from June to August in both 2019 and 2020. AMSR2 SID was converted into SIT using the hydrostatic equation [35, eq. (13)] with auxiliary data, such as snow/ice densities and snow depth, which are used in [34]. Given that SID comprises up to 90% of the total sea ice, the observation error of AMSR2 SIT is set at 0.43 m, matching the maximum observation error value of 0.38 m for AMSR2 SID [35]. The similarity between the maximum observational error of AMSR2 and the mean observational error of CS2 suggests that AMSR2 yields a more accurate SIT estimate. The snow depth and density estimates derived from the Lagrangian snow evolution scheme SnowModel-LG were used to convert SIT (SID) to SID (SIT) for both satellite products and model outputs [60], [61].

D. Data for Evaluation

The climate data record (CDR) of the satellite passive microwave-based (special sensor for microwave imager and sounder (SSMIS) daily SIC version 4 was used to validate the modeled SIE. This dataset is based on a combination of the bootstrap NASA-Team SIC algorithm. In addition, the pan-Arctic ice–ocean modeling and assimilation system (PIOMAS) SIT data were employed for validation [62]. Weekly averaged SIT product version 2.3 of CS2SMOS, which merges Level-2 preprocessed CryoSat-2 and Level-3 collated soil moisture ocean salinity (SMOS) data using an optimal interpolation scheme from the Alfred Wegener Institute, was also used to validate the updated SIT field [63]. For evaluation, both the model outputs and the satellite data were regridded onto a 1° rectilinear latitude/longitude grid system from the original grid system.

The BGEP ULS ice draft data from moorings and SIMB3 datasets[1] were used to validate the reanalysis data from the DA experiments. The measurement error of BGEP ULS SID is approximately 0.1 m [64], while that of SIMB3 is around 0.011 m [65]. Both in situ observation datasets exhibit higher accuracy compared with satellite-based data, with AMSR2 and CS2 exhibiting observational errors of about 0.43 m [35] and 0.41 m [41], respectively.

The SIMB3 buoys, which include those from Multidisciplinary Drifting Observatory for the Study of Arctic Climate (MOSAiC) and Dartmouth, were deployed. The Dartmouth buoys and moorings were mainly distributed in the Beaufort Sea, while those deployed in the Central Arctic Ocean by the MOSAiC expedition drifted to the Fram Strait along the transpolar drift stream (see Fig. S1).

BGEP ULS SID observations from moorings A (75°N, 150°W), B (78°N, 150°W), and D (74°N, 140°W) during 2019–2020 were used to validate the SID reanalyzed from the DA experiments. Since 2003, the BGEP moorings in the Beaufort Sea have continuously monitored the freshwater and heat content of the Arctic Ocean, including the solid freshwater flux, through SID observations. BGEP ULS data, measured at 1-s intervals, were processed into daily averages to assess the daily model SID.

The SIT measurements from the SIMB3 dataset were also used for validation. The SIMB3 was developed to improve the monitoring of mass balance with design features that increase reliability and survivability, simplify installation, and reduce costs. SIMB3 data can be accessed from Cryosphere Innovation.[2] The instruments used were MOSAiC 2019 #1—3, Dartmouth 2019 #1, and 2020 #1—2 to assess the simulated SIT during both the summer and winter seasons. The observation period of each SIMB3 buoy is detailed in Table S1. Given the deployment conditions of the SIMB3 buoys, which can only measure SIT up to 2.5 m thick and are restricted to deployment on flat sea ice in the subgrid, caution is necessary when interpreting comparisons with the model outputs averaged over the grid space. To minimize the systematic differences between the model outputs, which represent variability over a certain area, and the point measurements, SIMB3 data from analogous time frames and regions were integrated and then used to validate the overall performance of the model. The SIMB3 data were first processed onto a 1° rectilinear latitude/longitude grid, averaged

[1] [Online]. Available: https://www.cryosphereinnovation.com/simb3
[2] [Online]. Available: https://www.cryosphereinnovation.com/data

TABLE I
OVERVIEW OF EIGHT EXPERIMENTS UTILIZED TO ASSESS THE IMPACT OF SATELLITE-DERIVED SUMMER SIT DATA

Experiment name	Integration period	Assimilated data		
		CS2	CS2 (upsampled)	AMSR2
CTL19				
CS2_DA19	1 June 2019–31 May 2020	• (1 June 2019–31 August 2019)		
CS2up_DA19			• (1 June 2019–31 August 2019)	
AMSR2_DA19				• (1 June 2019–31 August 2019)
CTL20				
CS2_DA20	1 June 2020–31 May 2021	• (1 June 2020–31 July 2020)		
CS2up_DA20			• (1 June 2019–31 July 2020)	
AMSR2_DA20				• (1 June2020–31 August2019)

Duration indicated in parentheses represents the assimilation period for each assimilated SIT data.

over 15-day intervals, and area averaged within 10° and 2° domains in the x and y directions, respectively, to assess the corresponding model simulations.

In addition to reference environmental information at the grid scale at which the SIMB3 buoys are located, the following satellite-based datasets were employed: Snow depth obtained from SnowModel-LG distributed by the National Snow and Ice Data Center (NSIDC) and SIC from the Ocean and Sea-Ice Satellite Application Facility of the European Organization for the Exploitation of Meteorological Satellites (EUMETSAT). NSIDC ice-age data (EASE-grid sea-ice age, version 4) and brightness temperature at band 31 based on the moderate resolution imaging spectroradiometer/aqua surface reflectance daily L3 global 0.05° climate modeling grid (MYDCMG v061), were also used.

E. DA Experiments Design

Table I summarizes the different experiments and compares the impacts of satellite-derived summer SIT DA across various experiments with distinct SIT observations. "CTL" is a control experiment without the DA of summer SIT observations, where SIT is simulated by CICE5 driven by atmospheric and oceanic boundary conditions. It is important to note that CryoSat-2 data generally have low spatiotemporal resolutions, featuring an 80-km horizontal resolution and biweekly (twice per month) temporal resolution [35], [40]. To overcome these limitations, previous studies have enhanced the spatiotemporal resolution of data using methods, such as upsampling using distance-weighted average mapping or piecewise constant interpolation for spatial upscaling, and linear interpolation for temporal upscaling [40], [41]. The uncertainty of the upscaled CryoSat-2 was set at 0.41 m, consistent with that of raw data, to isolate the impact of observation density on the DA experimental results. In this study, two approaches were implemented to assimilate CryoSat-2. First, in alignment with prior research [40], [41], an experiment named "CS2up_DA" utilized spatiotemporally upsampled CryoSat-2 data. In this experiment, CryoSat-2 SIT, upscaled to a daily basis with a 25-km resolution matching that of AMSR2, was assimilated into the CICE5. Second, the unaltered CryoSat-2 SIT, which maintains the original biweekly SIT with 80-km spatial resolution referred to as "CS2_DA," was assimilated. For the DA of AMSR2-based SIT, the corresponding experiment is designated as "AMSR2_DA."

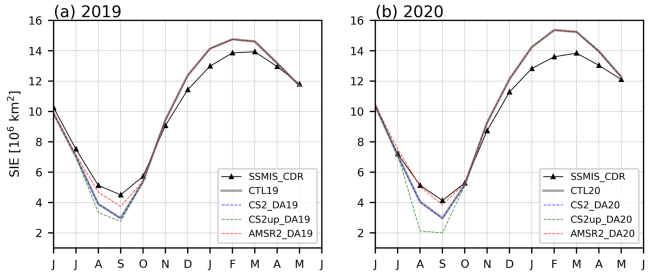

Fig. 1. Time series of monthly SIEs averaged over the Northern Hemisphere (50°–90°N) of SSMIS_CDR (black solid with triangles), CTL (gray solid), CS2_DA (blue dashed), CS2up_DA (green dashed), and AMSR2_DA (red dashed) from (a) June 2019 to May 2020 and (b) June 2020 to May 2021.

The experiments spanned from 1 June 2019 to 31 May 2020 and from 1 June 2020 to 31 May 2021. The sea-ice initial conditions for each experiment were derived from the sequential assimilation of winter L4 CryoSat-2 and L3 SMOS SIT data into CICE5, using the same boundary conditions as this study, from 2011 to 2020 [45]. Although satellite data were not assimilated beyond September in any of the experiments, the model predictions were kept until the subsequent winter and spring seasons to evaluate the impact of the summer SIT data on later periods.

III. RESULTS

A. Simulation Quality During the Boreal Summer

Fig. 1 displays the monthly averaged Arctic SIE, which is defined as the total area of all grid cells with SIC greater than 0.15 across the Northern Hemisphere. SIT DA experiments have little impact on the SIE simulation during the cold season because the thickness changes by SIT DA cannot affect new ice formation (see Section II-B). SIE simulations from June to August reveal distinct differences between CTL and DA experiments for both 2019 and 2020. The simulated SIE in CTL tended to exhibit underestimation from June to October compared with the satellite-derived observations. Notably, SIE with CS2_DA shows little deviation from SIE with CTL during the assimilated periods, indicating that the DA impact of CS2 on SIE is minimal. Conversely, AMSR2_DA demonstrates a significant improvement over CTL. AMSR2_DA effectively improved the underestimation of SIT in CTL in both the 2019 and 2020 experiments. In September 2020, both the SIEs with CTL and CS2_DA exhibited an underestimation of -1.1×10^6 km^2 compared with the SIE derived from the SSMIS CDR, whereas the simulated SIE with AMSR2_DA displayed a considerably reduced underestimation of -0.1×10^6 km^2 [see Fig. 1(b)]. Furthermore, CS2up_DA exhibited the lowest SIE for August–September in both 2019 and 2020, which could be attributed to the ice roughness-related negative bias in CS2 SIT over multiyear ice (MYI) regions [35], [40].

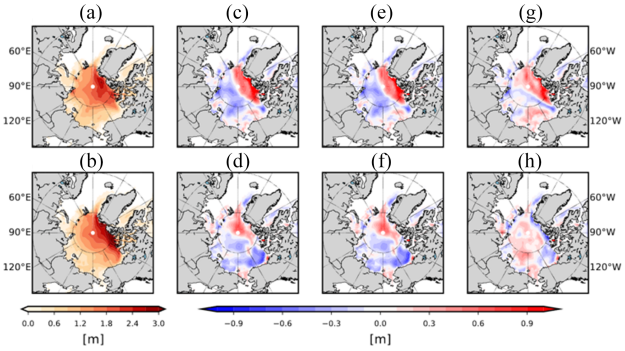

Fig. 2. Spatial distribution of mean SIT from PIOMAS (first column) and the differences of CTL (second column), CS2_DA (third column), and AMSR2_DA (fourth column) relative to PIOMAS during the periods of JJA 2019 (upper) and JJ 2020 (lower). (a) PIOMAS [JJA 2019]. (b) PIOMAS [JJA 2020]. (c) CTL19–(a). (d) CTL20–(b). (e) CS2_DA19–(a). (f) CS2_DA20–(b). (g) AMSR2_DA19–(a). (h) AMSR2_DA20–(b).

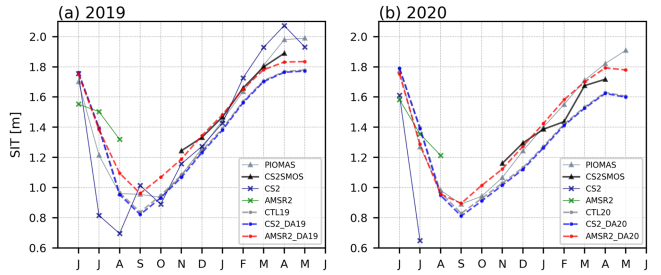

Fig. 3. Time series of monthly SITs over the Northern Hemisphere (50°–90°N) in PIOMAS (gray, solid with triangle), CS2SMOS (black, solid with triangle), CS2 (navy, solid with x marker), AMSR2 (green, solid with x marker), CTL (gray, dashed with dot marker), CS2_DA (blue, dashed with dot marker), and AMSR2_DA (red, dashed with dot marker) (a) from June 2019 to May 2020 and (b) from June 2020 to May 2021. (a) 2019. (b) 2020.

Our results are not likely to be consistent with those of the prior study [42], which demonstrated that the assimilation of upsampled CS2 data improved SIE simulation performance. However, it should be noted that the improvement using upsampled CS2 data in [42] was likely achieved by artificially amplifying observation errors to mitigate the underestimation issues of CS2. Because neither the CS2_DA nor CS2up_DA experiments demonstrated improvements over CTL, this study will focus solely on the results of the CS2_DA experiment going forward, rather than considering both experiments.

To examine the regional distribution of the simulated summer SIT, average SIT values for June–July–August (JJA) 2019 and June–July (JJ) 2020 were calculated across three experiments and PIOMAS reanalysis during the two periods (see Fig. 2). The reason for using different months to represent summer SIT in 2019 and 2020 is that CS2 data are available only up to July 2020. PIOMAS showed that SIT distributions predominantly exceeded 2.5 m in the western part of the central Arctic Ocean, where MYI is prevalent, thinning progressively toward the subpolar regions in both time frames [see Fig. 2(a) and (b)]. In 2019, CTL resulted in an overestimation of SIT in the western part of the Arctic Ocean and an underestimation in the eastern part compared with SIT from PIOMAS [see Fig. 2(c)]. In 2020, CTL overestimated SIT North of Greenland and underestimated SIT in the Beaufort Sea [see Fig. 2(d)]. Despite the assimilation of the CryoSat-2 summer SIT data, CS2_DA showed minimal improvement over CTL simulation during both periods of the experiment [see Fig. 2(e) and (f)]. In contrast, the DA of AMSR2 SIT effectively corrected the underestimation (overestimation) of the simulated SIT in CTL over the eastern Arctic Ocean (North of Greenland) in 2019 and over the Beaufort Sea (North of Greenland) in 2020 [see Fig. 2(g) and (h)]. Root-mean-square-difference analysis was used to quantify the differences between each model experiment and observations (see Figs. S2 and S3). The results show that AMSR2_DA led to a reduction in errors across the Arctic Ocean and demonstrated a statistically significant improvement over CS2_DA at the 99% confidence level (see Tables S2 and S3).

To understand the overall temporal evolution of SIT, the time series of SIT for the model experiments, the satellite summer SIT data used for assimilation, PIOMAS reanalysis, and CS2SMOS satellite data were analyzed (see Fig. 3). The seasonal cycle of the SIT is clearly illustrated in both reference datasets and model experiments. CS2 SIT displayed the largest amplitude of the seasonal cycle compared with other references and simulations, as indicated by the navy line with a marker "x" in Fig. 3. In contrast, AMSR2 showed a relatively weak melt signal compared with other products and simulations during the melt season, which is represented by the green line with a marker "x" in Fig. 3.

The simulation results exhibit a distinct contrast. In September, the SIT with AMSR2_DA was significantly thicker than the SITs with CTL and CS2_DA, despite AMSR2 SIT not being assimilated during this month. This difference was primarily attributed to the thicker SIT in AMSR2_DA during the rapid ice-melting season (see Fig. 3), which likely contributed to the improved simulation of SIE (see Fig. 1). During the subsequent ice-growing season from October to April, the evolution of the Arctic SIT indicates that the summer SIT DA influences the simulated SIT over the seasonal timescales. In contrast, SIE has a relatively short memory and can be quickly aligned with model climatology by boundary forcing. As the SIT during JJA extended into the freezing season (i.e., November to April), AMSR2_DA simulated thicker ice overall more closely resembling CS2SMOS and PIOMAS than the other experiments during both experimental periods. In CTL and CS2_DA, SIT undergoes excessive reduction, with CS2_DA showing slightly more underestimation due to its assimilation of CS2 data with thinner SIT values during summer. Conversely, AMSR2_DA significantly corrects these underestimations. This may be because the weaker decreasing rate of SIT in AMSR2 data more closely resembles PIOMAS compared with the pronounced seasonal reduction observed in CS2. This suggests that a more accurate summer SIT supports improved SIT simulations on seasonal timescales, with its positive impacts extending into the subsequent freezing season. In other words, the realistic summer SIT leads to the realistic simulation of SIT on seasonal timescales, with its positive impacts extending into the subsequent freezing season.

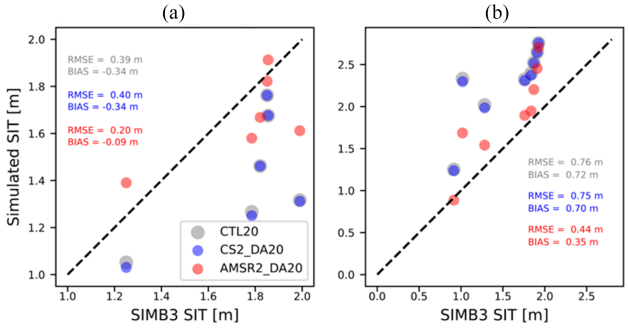

Fig. 4. Scatter plots of spatiotemporally averaged (a) Dartmouth_2019_#1 and (b) MOSAiC_2019_#3 SIMB3 SIT (x-axis) and the corresponding SITs with CTL20 (gray circle), CS2_DA20 (blue circle), and AMSR2_DA20 (red circle) simulations (y-axis) during June–July 2020. SIMB3 data were used by averaging over 15-day intervals and area averaging within 10° and 2° domains in the x and y directions, respectively, to assess the corresponding model simulations. (a) Dartmouth_2019_#1. (b) Dartmouth_2019_#3

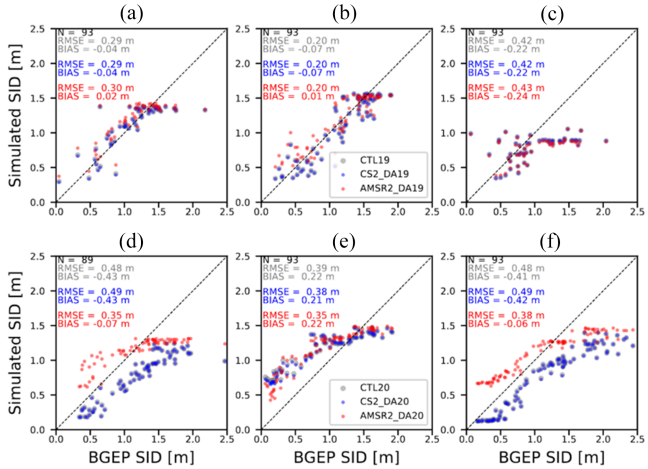

Fig. 5. Scatter plots of daily averaged SID from BGEP ULS 18a (left column), 18b (middle column), and 18d (right column) and the corresponding SIDs with CTL (gray circle), CS2_DA (blue circle), and AMSR2_DA (red circle) simulations (y-axis) during JJA 2019 (upper panel) and 2020 (lower panel). (a) 18a [JJA 2019]. (b) 18b. (c) 18d. (d) 18a [JJA 2020]. (e) 18b. (f) 18d.

The interpretation of this diagnostic for the assimilated observations requires caution because both satellite products experience some grid points with missing values due to algorithmic failures. SIT with CS2 may be overestimated during the early growth season due to the exclusion of new thin sea ice in the marginal ice zone (MIZ) at the end of September. A known limitation of the summer radar freeboard algorithm is its difficulty in accurately retrieving thin ice [39]. Conversely, the Arctic-averaged AMSR2 SIT data may show underestimated values in early June, resulting from missing points in thick sea-ice areas where the melt signal is not pronounced and may be overestimated in late August due to algorithmic limitations that affect ice drift tracking in the MIZs [35]. However, these missing points did not impact the DA experiments since they were excluded from the DA process.

To enhance the validation rigor, the fidelity of the reanalysis fields was verified by comparing it with independent in situ observations. Initially, the quality of the simulated SIT was assessed using the available SIMB3 data from June to July 2020, specifically from the Dartmouth_2019_#1 and MOSAiC_2019_#3 buoys (see Fig. 4). Given the limitations related to spatial resolution in the ability of the model to represent the variability observed at point measurements, the SIMB3 SIT data were spatiotemporally averaged to assess the results of the corresponding experiments, as outlined in Section II-D. The underestimated SITs in both CTL and CS2_DA against Dartmouth_2019_#1 buoy were effectively corrected in AMRS2_DA [see Fig. 4(a)]. While CTL and CS2_DA simulations exhibit negative biases of approximately -0.3 m, AMSR2_DA simulation demonstrates a significantly better agreement with the observations, displaying a smaller bias of approximately -0.1 m. In addition, the RMSE in AMSR2_DA simulation exhibits a significantly lower value of approximately 50% compared with the other experiments. It is important to note that the pointwise Dartmouth_2019_#1 buoy is likely an underestimation of the representative SIT in the model grid space due to the high brightness temperatures and the presence of MYI for two or more years since the deployment of the buoy predominantly characterized the grid (see Fig. S4d). Furthermore, Dartmouth_2019_#1 estimated an SIT of approximately half that of CS2SMOS, which is approximately 2 m during the ice-growing season (i.e., September–December 2019). Even when considering the potential of underestimation in the Dartmouth_2019_#1 buoy, the improvement seen in AMSR2_DA appears definite, given that the model outputs are generally thinner than those of the buoy.

The modeled SIT in both CTL and CS2_DA shows overestimation against the MOSAiC_2019_#3 buoy, with bias values exceeding 0.75 m. However, this overestimation was significantly reduced by AMSR2_DA [see Fig. 4(b)]. This is generally consistent with the spatial distribution of the differences between the experiments and PIOMAS (see Fig. 2). The MOSAiC_2019_#3 buoy was considered to represent a relatively accurate SIT for its grid cell at the time of deployment. The grid traversed by this buoy features predominantly young sea ice, typically two years old or less, and exhibits relatively low brightness temperatures [66]. The SIT measured by the buoy during winter (i.e., from November 2019 to January 2020) was similar to that of CS2SMOS (see Fig. S4c). However, it is important to note that the estimates from June to July 2020, as measured by the buoy, may have been somewhat overestimated due to slower SIT growth related to the ice growth–ice thickness negative feedback [67], compared with CS2SMOS. Despite this consideration, AMSR2_DA demonstrated a noticeable improvement over the other experiments because its model outputs were generally thicker than those of the buoy. The comparison of simulated SIT at the model grid point closest to the observation site with the daily averaged values of the two buoys further supports the enhancement achieved by AMSR2_DA (see Fig. S5).

The SIT simulations were also assessed using the daily averaged SID obtained from the BGEP ULS (see Fig. 5). To convert the modeled SIT into an SID, the reverse procedure used to convert an AMSR2 SID to SIT (refer to Section II-A) was applied in this study. During JJA 2019, the three experiments showed a fairly accurate representation of BGEP ULS sites 18a and 18b,

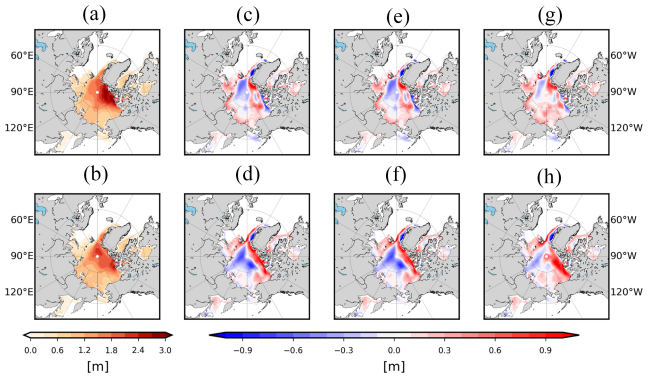

Fig. 6. Spatial distributions of mean SIT from CS2SMOS (first column) and difference in SIT between CTL (second column), CS2_DA (third column), and AMSR2_DA (fourth column) and CS2SMOS during December–February 2019/20 (upper) and 2020/21 (lower). (a) CS2SMOS [DJF 2019]. (b) CS2SMOS [DJF 2020]. (c) CTL19–(a). (d) CTL20–(b). (e) CS2_DA19–(a). (f) CS2_DA20–(b). (g) AMSR2_DA19–(a). (h) AMSR2_DA20–(b).

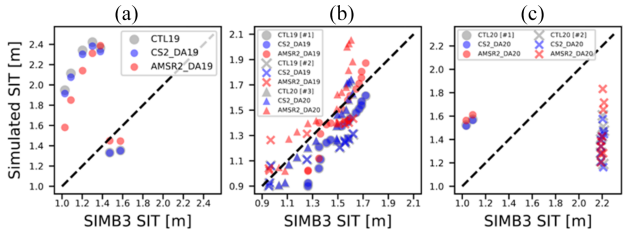

Fig. 7. Scatter plots of spatiotemporally averaged SITs from (a) Dartmouth_2019_1, (b) MOSAiC_2019_1–3, and (c) Dartmouth_2020_1–2 SIMB3 (x-axis) and the corresponding SITs with CTL (gray circle), CS2_DA (blue circle), and AMSR2_DA (red circle) simulations (y-axis) during the periods of December–February (a) and (b) 2019/20 and (c) 2020/21. SIMB3 data were used by averaging over 15-day intervals and area averaging within 10° and 2° domains in the x and y directions, respectively, to assess the corresponding model simulations. (a) Dartmouth_2019_#1 [19]. (b) MOSAiC_2019_#1–3 [19]. (c) Dartmouth_2020_#1–2 [20].

but an underestimation for site 18d. The simulated SIDs from the three experiments at the BGEP site are almost the same [see Fig. 5(a)–(c)]. Conversely, in the summer of 2020, AMSR2_DA effectively reduced the RMSEs and negative biases of SID in CTL and CS2_DA at sites a and d near the coastline [see Fig. 5(d) and (f)]. At site 18b, as the sea ice thins, AMSR2_DA showed greater similarity to the observations compared with the others during JJA 2020 [see Fig. 5(e)].

However, during JJA 2020, AMSR2_DA did not adequately capture the observed decline in sea ice because the SID estimated from AMSR2 did not sufficiently capture the decline observed in the BGEP ULS (see Fig. S7), unlike in 2019 (see Fig. S6).

Conversely, CS2_DA generally depicted thinner sea ice than the observations (see Fig. 5), with CS2 SIT data indicating the overall thicker sea ice and a weaker melting trend than that of the BGEP_ULS (see Figs. S6 and S7). This might indicate that the information concerning CS2 was not adequately reflected in CS2_DA.

B. Simulation Quality During the Subsequent Growing Season

The summer SIT can significantly influence the simulation of sea-ice conditions during the subsequent ice-growing season. For example, thinner sea ice enhances heat transfer from the warmer bottom to the colder surface layer, accelerating sea-ice growth during the growing season [68]. This phenomenon is known as the negative feedback between ice thickness and ice growth [69]. This suggests that the underestimation of SIT in CTL and CS2_DA can lead to amplified variations in sea-ice conditions. This section explores how summer SIT DA impacts the simulation results during the freezing season.

Fig. 6 displays the simulated SIT during the subsequent boreal winter season following the SIT DA for the experiments conducted in 2019 and 2020 [December–January–February (DJF) 2019/20 for 2019 experiments and DJF 2020/21 for 2020 experiments]. The differences in SIT between CS2SMOS and each experiment reveal that the underestimations in SIT for CTL and CS2_DA are primarily located in the central Arctic Ocean during both experimental periods [see Fig. 6(c)–(f)]. These underestimations for CTL and CS2_DA are significantly reduced for AMSR2_DA, although some overestimations remain for the Canadian Archipelago, Barents Sea, and Pacific sectors [see Fig. 6(g) and (h)]. Using PIOMAS as a reference, the results show that AMSR2_DA effectively addresses the underestimated SIT in CTL and CS2_DA (see Fig. S8). The experimental differences in winter SIT are most pronounced near the central Arctic Ocean.

The reason AMSR2_DA outperforms CS2_DA in SIE and SIT predictions is its ability to produce more accurate SIT reanalysis. CS2 data, which measure ice freeboard height using a radar altimeter, exhibit higher uncertainties in thick ice regions with significant surface roughness caused by ice deformation, such as ridging [34]. In contrast, AMSR2 data, which estimate ice draft using passive microwave sensors, avoid these issues and achieve higher observational accuracy in thick sea-ice regions. This advantage is reflected in the DA experiments, where AMSR2_DA simulates a more reliable SIT reanalysis compared with other experiments, resulting in superior prediction performance. Thus, the improvement in AMSR2_DA is attributed to the systematic difference between two satellite data.

From December 2019 to January and February 2020, all experiments produced simulations of thicker SIT than the observed SIT by Dartmouth_2019_#1, which was less than 1.4 m [see Fig. 7(a)]. In comparison with the other experiments, AMSR2_DA most accurately represented observations in thin sea-ice conditions. When the observed Dartmouth_2019_#1 SIT reached 1.5 m or greater, all the simulated SITs exhibited a sudden drop, resulting in values relatively similar to the observations. This phenomenon is likely due to abrupt regional gradients in the simulated SIT along the southward drift path of the buoy, as indicated by a dipole pattern of differences between the simulations and CS2SMOS near 140°–130°W and 75°–80°N [see Fig. 6(c), (e), and (g)]. The RMSE and bias were also larger, with AMSR2_DA having the smallest, followed by CS2_DA and CTL (see Table II). In the trajectories of the MOSAiC buoys (MOSAiC_2019_#1–3 in Table II), the simulated SIT in AMSR2_DA was consistently thicker than the SITs in CTL and CS2_DA [see Fig. 7(b)], with AMSR2_DA showing a 26%

TABLE II
RMSEs AND BIASES BETWEEN THE SIMB3 SIT AND SIT WITH EACH SIMULATION DURING D(0)JF(+1) SEASON FOR THE YEARS OF 2020 (DARTMOUTH_2019_#1 AND MOSAiC_2019_#1–3) AND 2021 (DARTMOUTH_2020_#1–2)

OBS platform	Diagnostics	CTL19/20	CS2_DA19/20	AMSR2_DA19/20
Dartmouth_2019_#1 (2020)	RMSE (m)	0.89	0.85	**0.74**
	BIAS (m)	0.69	0.66	**0.59**
MOSAiC_2019_#1 (2020)	RMSE (m)	0.22	0.22	**0.12**
	BIAS (m)	−0.20	−0.20	**−0.03**
MOSAiC_2019_#2 (2020)	RMSE (m)	0.24	0.24	**0.16**
	BIAS (m)	−0.19	−0.19	**−0.03**
MOSAiC_2019_#3 (2020)	RMSE (m)	0.11	**0.11**	0.1372
	BIAS (m)	−0.09	−0.09	**0.08**
MOSAiC_2019_#1–3 (2020)	RMSE (m)	0.19	0.19	**0.14**
	BIAS (m)	−0.16	−0.16	**0.01**
Dartmouth_2020_#1 (2021)	RMSE (m)	0.49	**0.48**	0.52
	BIAS (m)	0.49	**0.48**	0.52
Dartmouth_2020_#2 (2021)	RMSE (m)	0.83	0.84	**0.77**
	BIAS (m)	−0.82	−0.83	**−0.74**
Dartmouth_2020_#1–2 (2021)	RMSE (m)	0.77	0.79	**0.73**
	BIAS (m)	−0.58	−0.59	**−0.51**

Boldface indicates the lowest RMSE and absolute value of bias.

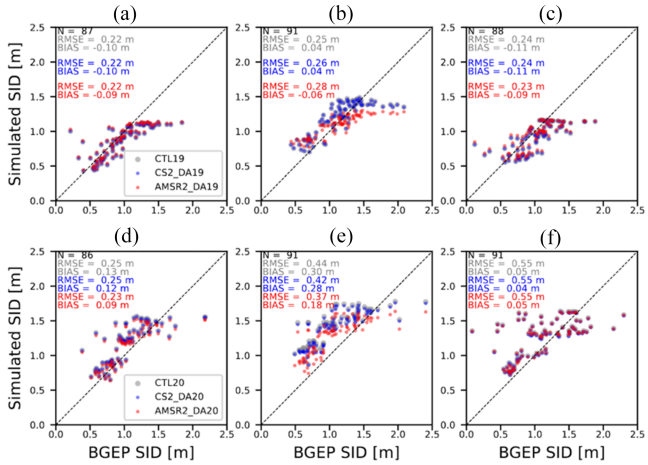

Fig. 8. Scatter plots of daily averaged SID observed by BGEP ULS 18a (left column), 18b (middle column), and 18d (right column) and the corresponding SID with CTL (gray circle), CS2_DA (blue circle), and AMSR2_DA (red circle) simulations (y-axis) during D(0)JF(+1) 2019 (upper panel) and 2020 (lower panel). (a) 18a [DJF 2019]. (b) 18b. (c) 18d. (d) 18a [DJF 2020]. (e) 18b. (f) 18d.

lower RMSE and a 94% lower bias, respectively (see Table II). Given that the MOSAiC buoys provided a relatively accurate representation of the grid-scale satellite SIT during winter [65], AMSR2_DA appeared to offer a more realistic SIT simulation (see Figs. S4a–c).

Regarding the Dartmouth_2020_#1 and Dartmouth_2020_#2 buoys, which recorded a wide range of SIT from 1.05 to 2.24 m, it was generally observed that the modeled SIT lies between thinner Dartmouth_2020_#1 and the thicker Dartmouth_2020_#2 [see Fig. 7(c)]. The model experiments exhibit growth similar to those observed by Dartmouth_2020_#1 but generally overestimate SIT. Given that Dartmouth_2020_#1 recorded an SIT comparable with satellite-derived grid-scale SIT (see Fig. S4e), it can be inferred that CS2_DA provided the most accurate simulation of SIT in the region where Dartmouth_2020_#1 was deployed, exhibiting minimum RMSE and bias (see Table II). Conversely, Dartmouth_2020_#2 recorded thick sea ice exceeding 2 m with only slight temporal changes. In comparison, CS2_DA and CTL exhibit growing SIT ranging from 1.1 to 1.6 m, and AMSR2 ranges from 1.2 to 1.8 m. AMSR2_DA closely aligns with Dartmouth_2020_#2; however, since this buoy recorded SIT that is thicker compared with CS2SMOS (see Fig. S4f), interpretation must be approached with caution. Conversely, in the comparative analysis of the six buoys averaged over the day, AMSR2_DA generally showed improved quality compared with the other experiments (see Fig. S9).

The quality evaluation of the experiments using the BGEP ULS SID data is explored further (see Fig. 8). During DJF 2019, while AMSR2_DA showed some improvement in bias at sites 18a and 18d compared with the other experiments, the differences among the experiments were not particularly significant [see Fig. 8(a) and (c)]. At site 18b, unlike sites 18a and 18b, AMSR2_DA exhibits a narrower range of SIT than the other experiments, indicating slower SIT growth [see Fig. 8(b)]. This site had the thickest SIT in AMSR2_DA compared with the SITs in CTL and CS2_DA during JJA 2019 [see Fig. 5(b)]. Interestingly, the significant underestimation in CTL and CS2_DA during JJA 2020 at sites 18a and 18d and the enhancement observed in AMSR2 [see Fig. 5(d) and (f)] did not continue into the DJF season; instead, the bias was reversed [see Fig. 8(d) and (f)]. At sites 18a and 18b, AMSR2_DA exhibits reduced RMSE and bias compared with the other experiments [see Fig. 8(d) and (e)], whereas at site 18d, there is little difference observed. Notably, at site 18b, the smallest difference in bias and RMSE between experiments was observed in JJA 2020 [see Fig. 5(e)], whereas the largest difference occurs in DJF 2020 [see Fig. 8(e)]. Given the strong high-pressure conditions that typically result in prevailing windy conditions over the Beaufort Sea (i.e., Beaufort High [70]), it is plausible that the largest difference can be attributed to the drift of sea ice from other regions. This suggests that, although the enhancement of simulated summer SIT through assimilation yields positive effects, the effects vary considerably across regions within seasonal timescales.

IV. SUMMARY AND DISCUSSION

Recent advancements in satellite-derived summer SIT products offer opportunities for creating more reliable reanalysis data through DA and exploring their impacts on sea-ice predictions over seasonal timescales. This study conducted DA experiments by assimilating summer SIT retrieved from CS2 [34] and AMSR2 [35] during JJA in 2019 and 2020. These experiments, which incorporated two datasets, yielded distinct results both concurrently and over seasonal timescales. During the summer season, the simulated SIEs in CTL and CS2_DA were underestimated compared with the SSMIS SIE with a generally thin SIT, particularly in the eastern Arctic Ocean. The DA experiment using spatiotemporally upscaled CS2 exhibited biases similar to or more significant than those observed in CS2_DA. In contrast, the DA of AMSR2 SIT corrected these errors and produced a realistic SIE and SIT reanalysis, which was validated with the SSMIS SIE and PIOMAS SIT data

during the melt season. Further evaluation of the SIT reanalysis using the SIMB3 buoys and BGEP ULS moorings showed that AMSR2_DA improved the overall accuracy and day-to-day variation of the simulated SIT compared with CS2_DA and CTL. The changes in the summer SIT simulations influenced SIT evolution on the seasonal timescale. The assimilation of AMSR2 data resulted in thicker sea ice during JJA, which was sustained during the subsequent growth season, thus offsetting the underestimation in CTL and CS2_DA and achieving a more realistic reanalysis.

The significant difference in how the DA of the two satellite-derived summer SIT datasets updates the model background field carries crucial implications. The systematic underestimation in CS2 over the central Arctic Ocean can intensify the underestimation in CTL. Therefore, this aspect must be considered when using CS2 to initialize numerical models and/or reconstruct historical data through DA. For instance, Song et al. [71] demonstrated that assimilating CryoSat-2 SIT data during summer could effectively reduce forecast errors in the ice-edge regions during the melt season by artificially inflating the observational errors in thick ice regions with large negative biases. This suggests that, although CS2 exhibits a significant negative systematic error over the central Arctic Ocean, its observations in the MIZs positively influence the predictions.

Assimilating AMSR2 SIT improves the background state more effectively than CS2 SIT due to AMSR2s less negative bias and higher accuracy. This accuracy is derived from AMSR2 estimating SIT from SID, which represents about 90% of SIT, while CS2 uses freeboard, which accounts for only 10% [35], [72]. The smaller magnitude of freeboard introduces greater uncertainty in SIT estimates. By assimilating AMSR2 SIT, sea-ice condition predictions improve, with benefits lasting at least until September.

Although the summer SIT data from AMSR2 exhibit relatively higher quality than those from CS2, as validated against independent BGEP ULS and buoy measurements [35], the Arctic basin-scale distribution of the two products has not been examined. For instance, AMSR2-derived SIT is generally thicker than that from CS2, except in the Barents–Kara Seas during JJA 2019 and JJ 2020, where AMSR2 reports substantially thinner SIT in CS2 (see Fig. S10).

Both AMSR2 and CS2 SIT datasets require further refinement. AMSR2 SID is based on the correlation between the brightness temperature from AMSR2 and SID measured by BGEP ULS during the melt season. To define the melt period SID, the SID at the melt-onset date (D_{on}) must be detected, employing a procedure heavily reliant on assumptions derived from the algorithm used to estimate winter ice freeboard from passive microwave satellite measurements [35], [73]. Landy et al. [34] derived summer SIT using CryoSat-2 by applying a melting correction to the ice freeboard during the melt season. However, the accuracy of radar altimetry is compromised by the presence of surface meltwater and the corresponding percolated waters within a sea-ice system, which obstructs the detection of the snow–ice interface. Although satellite-based summer SIT estimates have considerable scope for enhancement, this study demonstrates that assimilating accurate SIT significantly improves the simulation performance of sea-ice conditions on seasonal timescales.

Similar to the findings from several studies that assimilated SMOS SITs in winter, where only thin sea ice of high accuracy is employed [7], [14], [43], DA using summer SIT with robust quality is likely to enhance prediction performance. Given the reported positive impacts of CS2 DA on the simulation and prediction effectiveness in regions with thin sea ice [41], [71], CS2 SIT over MIZs may exhibit higher accuracy. This indicates that CS2 and AMSR2 could improve sea-ice prediction performance when their regional advantages are selectively utilized, similar to the way complementary features are incorporated during the DA of winter CryoSat-2 and SMOS [14], [43], [45]. Future studies aim to explore the effects of assimilating both products, taking into account the regional quality of observations.

Acknowledgment

The authors would like to thank the National Snow and Ice Data Center (NSIDC) for the climate data record of passive microwave sea-ice concentration version 4 data, the Polar Science Center (PSC) for reanalyzed sea-ice thickness from PIOMAS, Alfred Wegenner Institute (AWI) for CS2SMOS sea-ice thickness, National Oceanic and Atmospheric Administration (NOAA) for NCEP-DOE Reanalysis 2 with Global T62 Gaussian grid and OISST version 2 high-resolution dataset with 0.25° latitude/longitude global grid to prescribe atmospheric/oceanic data as the boundary condition to run CICE5, and British Antarctic Survey Polar Data Center for the year-round CryoSat-2 sea-ice thickness data, Kim et al. [35] for AMSR2-derived sea-ice draft data, Woods Hole Oceanographic Institution (WHOI) for the BGEP ULS-measured sea-ice draft data, Cryosphere Innovation for SIMB3-measured sea-ice thickness, NSIDC for the SnowModel-LG data, the European Organization for the Exploitation of Meteorological Satellites (EUMETSAT) for the OSISAF SIC data, and the Land Processes Distributed Active Archive for the MODIS-retrieved brightness temperature data.

References

[1] R. Kwok, "Arctic sea ice thickness, volume, and multiyear ice coverage: Losses and coupled variability (1958-2018)," *Environ. Res. Lett.*, vol. 13, no. 10, 2018, Art. no. 105005, doi: 10.1088/1748-9326/aae3ec.

[2] J. Stroeve and D. Notz, "Changing state of Arctic sea ice across all seasons," *Environ. Res. Lett.*, vol. 13, Sep. 2018, Art. no. 103001, doi: 10.1088/1748-9326/aade56.

[3] J. Cohen, L. Agel, M. Barlow, C. I. Garfinkel, and I. White, "Linking Arctic variability and change with extreme winter weather in the United States," *Science*, vol. 373, no. 6559, pp. 1116–1121, Sep. 2021, doi: 10.1126/science.abi9167.

[4] D. Coumou, G. Di Capua, S. Vavrus, L. Wang, and S. Wang, "The influence of Arctic amplification on mid-latitude summer circulation," *Nature Commun.*, vol. 9, Dec. 2018, Art. no. 2959, doi: 10.1038/s41467-018-05256-8.

[5] R. Jaiser, K. Dethloff, D. Handorf, A. Rinke, and J. Cohen, "Impact of sea ice cover changes on the Northern Hemisphere atmospheric winter circulation," *Tellus A, Dyn. Meteorol. Oceanogr.*, vol. 64, no. 1, 2012, Art. no. 11595, doi: 10.3402/tellusa.v64i0.11595.

[6] W. N. Meier et al., "Arctic sea ice in transformation: A review of recent observed changes and impacts on biology and human activity," *Rev. Geophys.*, vol. 52, pp. 185–217, Sep. 2014, doi: 10.1002/2013RG000431.

[7] Z. Chen, J. Liu, M. Song, Q. Yang, and S. Xu, "Impacts of assimilating satellite sea ice concentration and thickness on Arctic sea ice prediction in the NCEP climate forecast system," *J. Climate*, vol. 30, no. 21, pp. 8429–8446, 2017, doi: 10.1175/JCLI-D-17-0093.1.

[8] F. Massonnet, T. Fichefet, and H. Goosse, "Prospects for improved seasonal Arctic sea ice predictions from multivariate data assimilation," *Ocean Model.*, vol. 88, pp. 16–25, 2015, doi: 10.1016/j.ocemod.2014.12.013.

[9] M. Kimmritz, F. Counillon, C. M. Bitz, F. Massonnet, I. Bethke, and Y. Gao, "Optimising assimilation of sea ice concentration in an Earth system model with a multicategory sea ice model," *Tellus A, Dyn. Meteorol. Oceanogr.*, vol. 70, no. 1, pp. 1–23, 2018, doi: 10.1080/16000870.2018.1435945.

[10] L. Ponsoni, F. Massonnet, T. Fichefet, M. Chevallier, and D. Docquier, "On the timescales and length scales of the Arctic sea ice thickness anomalies: A study based on 14 reanalyses," *Cryosphere*, vol. 13, no. 2, pp. 521–543, Feb. 2019, doi: 10.5194/tc-13-521-2019.

[11] E. Blanchard-Wrigglesworth, K. C. Armour, C. M. Bitz, and E. Deweaver, "Persistence and inherent predictability of Arctic sea ice in a GCM ensemble and observations," *J. Climate*, vol. 24, no. 1, pp. 231–250, Jan. 2011, doi: 10.1175/2010JCLI3775.1.

[12] M. M. Holland, D. A. Bailey, and S. Vavrus, "Inherent sea ice predictability in the rapidly changing Arctic environment of the community climate system model, version 3," *Climate Dyn.*, vol. 36, no. 7, pp. 1239–1253, Apr. 2011, doi: 10.1007/s00382-010-0792-4.

[13] R. W. Lindsay, J. Zhang, A. J. Schweiger, and M. A. Steele, "Seasonal predictions of ice extent in the Arctic Ocean," *J. Geophysical Res. Oceans*, vol. 113, no. 2, Feb. 2008, Art. no. 5124, doi: 10.1029/2007JC004259.

[14] D. Mignac, M. Martin, E. Fiedler, E. Blockley, and N. Fournier, "Improving the met office's forecast ocean assimilation model (FOAM) with the assimilation of satellite-derived sea-ice thickness data from CryoSat-2 and SMOS in the Arctic," *Quart. J. Roy. Meteorol. Soc.*, vol. 148, no. 744, pp. 1144–1167, Apr. 2022, doi: 10.1002/qj.4252.

[15] E. K. Fiedler et al., "Assimilation of sea ice thickness derived from CryoSat-2 along-track freeboard measurements into the met office's forecast ocean assimilation model (FOAM)," *Cryosphere*, vol. 16, no. 1, pp. 61–85, Jan. 2022, doi: 10.5194/tc-16-61-2022.

[16] E. W. Blockley and K. A. Peterson, "Improving met office seasonal predictions of Arctic sea ice using assimilation of CryoSat-2 thickness," *Cryosphere*, vol. 12, no. 11, pp. 3419–3438, 2018, doi: 10.5194/tc-12-3419-2018.

[17] L. Kaleschke, X. Tian-Kunze, N. Maaß, M. Mäkynen, and M. Drusch, "Sea ice thickness retrieval from SMOS brightness temperatures during the Arctic freeze-up period," *Geophys. Res. Lett.*, vol. 39, no. 5, 2012, Art. no. L05501, doi: 10.1029/2012GL050916.

[18] X. Tian-Kunze et al., "SMOS-derived thin sea ice thickness: Algorithm baseline, product specifications and initial verification," *Cryosphere*, vol. 8, no. 3, pp. 997–1018, 2014, doi: 10.5194/tc-8-997-2014.

[19] R. L. Tilling, A. Ridout, and A. Shepherd, "Estimating Arctic sea ice thickness and volume using CryoSat-2 radar altimeter data," *Adv. Space Res.*, vol. 62, no. 6, pp. 1203–1225, 2018, doi: 10.1016/j.asr.2017.10.051.

[20] R. L. Tilling, A. Ridout, and A. Shepherd, "Near-real-time Arctic sea ice thickness and volume from CryoSat-2," *Cryosphere*, vol. 10, no. 5, pp. 2003–2012, 2016, doi: 10.5194/tc-10-2003-2016.

[21] J. Zeng, Q. Yang, X. Li, X. Yuan, M. Bushuk, and D. Chen, "Reducing the spring barrier in predicting summer Arctic sea ice concentration," *Geophys. Res. Lett.*, vol. 50, no. 8, Apr. 2023, Art. no. e2022GL102115, doi: 10.1029/2022GL102115.

[22] M. Bushuk, M. Winton, D. B. Bonan, E. Blanchard-Wrigglesworth, and T. L. Delworth, "A mechanism for the Arctic sea ice spring predictability barrier," *Geophys. Res. Lett.*, vol. 47, no. 13, Jul. 2020, Art. no. e2020GL088335, doi: 10.1029/2020GL088335.

[23] D. B. Bonan, M. Bushuk, and M. Winton, "A spring barrier for regional predictions of summer Arctic sea ice," *Geophys. Res. Lett.*, vol. 46, no. 11, pp. 5937–5947, Jun. 2019, doi: 10.1029/2019GL082947.

[24] J. J. Day, S. Tietsche, and E. Hawkins, "Pan-Arctic and regional sea ice predictability: Initialization month dependence," *J. Climate*, vol. 27, no. 12, pp. 4371–4390, 2014, doi: 10.1175/JCLI-D-13-00614.1.

[25] S. Tietsche et al., "Seasonal to interannual Arctic sea ice predictability in current global climate models," *Geophys. Res. Lett.*, vol. 41, no. 3, pp. 1035–1043, 2014, doi: 10.1002/2013GL058755.

[26] A. A. Petty et al., "Skillful spring forecasts of September Arctic sea ice extent using passive microwave sea ice observations," *Earths Future*, vol. 5, no. 2, pp. 254–263, Feb. 2017, doi: 10.1002/2016EF000495.

[27] C. Brunette, B. Tremblay, and R. Newton, "Winter coastal divergence as a predictor for the minimum sea ice extent in the Laptev sea," *J. Climate*, vol. 32, no. 4, pp. 1063–1080, Feb. 2019, doi: 10.1175/JCLI-D-18-0169.1.

[28] D. Schröder, D. L. Feltham, D. Flocco, and M. Tsamados, "September Arctic sea-ice minimum predicted by spring melt-pond fraction," *Nature Climate Change*, vol. 4, no. 5, pp. 353–357, 2014, doi: 10.1038/nclimate2203.

[29] M. L. Kapsch, R. G. Graversen, T. Economou, and M. Tjernström, "The importance of spring atmospheric conditions for predictions of the Arctic summer sea ice extent," *Geophys. Res. Lett.*, vol. 41, no. 14, pp. 5288–5296, Jul. 2014, doi: 10.1002/2014GL060826.

[30] E. Blanchard-Wrigglesworth and C. M. Bitz, "Characteristics of Arctic sea-ice thickness variability in GCMs," *J. Climate*, vol. 27, no. 21, pp. 8244–8258, 2014, doi: 10.1175/JCLI-D-14-00345.1.

[31] D. G. Babb, J. C. Landy, D. G. Barber, and R. J. Galley, "Winter sea ice export from the Beaufort sea as a preconditioning mechanism for enhanced summer melt: A case study of 2016," *J. Geophys. Res. Oceans*, vol. 124, no. 9, pp. 6575–6600, Sep. 2019, doi: 10.1029/2019JC015053.

[32] J. Williams, B. Tremblay, R. Newton, and R. Allard, "Dynamic preconditioning of the minimum September sea-ice extent," *J. Climate*, vol. 29, no. 16, pp. 5879–5891, 2016, doi: 10.1175/JCLI-D-15-0515.1.

[33] P. Itkin and T. Krumpen, "Winter sea ice export from the Laptev sea preconditions the local summer sea ice cover and fast ice decay," *Cryosphere*, vol. 11, no. 5, pp. 2383–2391, Oct. 2017, doi: 10.5194/tc-11-2383-2017.

[34] J. C. Landy et al., "A year-round satellite sea-ice thickness record from CryoSat-2," *Nature*, vol. 609, no. 7927, pp. 517–522, Sep. 2022, doi: 10.1038/s41586-022-05058-5.

[35] J. M. Kim et al., "Estimation of summer pan-Arctic ice draft from satellite passive microwave observations," *Remote Sens. Environ.*, vol. 295, Sep. 2023, Art. no. 113662, doi: 10.1016/j.rse.2023.113662.

[36] A. A. Petty, N. Keeney, A. Cabaj, P. Kushner, and M. Bagnardi, "Winter Arctic sea ice thickness from ICESat-2: Upgrades to freeboard and snow loading estimates and an assessment of the first three winters of data collection," *Cryosphere*, vol. 17, no. 1, pp. 127–156, Jan. 2023, doi: 10.5194/tc-17-127-2023.

[37] C. Nab, R. Mallett, C. Nelson, J. Stroeve, and M. Tsamados, "Optimising interannual sea ice thickness variability retrieved from CryoSat-2," *Geophys. Res. Lett.*, vol. 51, no. 21, Nov. 2024, Art. no. e2024GL111071, doi: 10.1029/2024GL111071.

[38] F. Hernandez-Macia, C. Gabarro, G. S. Gomez, and M. J. Escorihuela, "A machine learning approach on SMOS thin sea ice thickness retrieval," *IEEE J. Sel. Topics Appl. Earth Observ. Remote Sens.*, vol. 17, pp. 10752–10758, May 2024, doi: 10.1109/JSTARS.2024.3406921.

[39] G. Dawson et al., "A 10-year record of Arctic summer sea ice freeboard from CryoSat-2," *Remote Sens. Environ.*, vol. 268, Jan. 2022, Art. no. 112744, doi: 10.1016/j.rse.2021.112744.

[40] C. Min et al., "Improving Arctic sea-ice thickness estimates with the assimilation of CryoSat-2 summer observations," *Ocean-Land-Atmos. Res.*, vol. 2, Jan. 2023, Art. no. 0025, doi: 10.34133/olar.0025.

[41] Y. F. Zhang et al., "Improvements in September Arctic sea ice predictions via assimilation of summer CryoSat-2 sea ice thickness observations," *Geophys. Res. Lett.*, vol. 50, no. 24, Dec. 2023, Art. no. e2023GL105672, doi: 10.1029/2023GL105672.

[42] R. Song, L. Mu, S. N. Loza, F. Kauker, and X. Chen, "Assimilating summer sea-ice thickness observations improves Arctic sea-ice forecast," *Geophys. Res. Lett.*, vol. 51, no. 13, Jul. 2024, Art. no. e2024GL110405, doi: 10.1029/2024GL110405.

[43] L. Mu et al., "Improving sea ice thickness estimates by assimilating CryoSat-2 and SMOS sea ice thickness data simultaneously," *Quart. J. Roy. Meteorol. Soc.*, vol. 144, no. 711, pp. 529–538, 2018, doi: 10.1002/qj.3225.

[44] J. G. Lee and Y. G. Ham, "Satellite-based data assimilation system for the initialization of Arctic sea ice concentration and thickness using CICE5," *Front. Climate*, vol. 4, Mar. 2022, Art. no. 02652, doi: 10.3389/fclim.2022.797733.

[45] J.-G. Lee and Y.-G. Ham, "Impact of satellite thickness data assimilation on bias reduction in Arctic sea ice concentration," *NPJ Climate Atmos. Sci.*, vol. 6, no. 1, Dec. 2023, Art. no. 73, doi: 10.1038/s41612-023-00402-6.

[46] D. Mignac, C. A. S. Tanajura, A. N. Santana, L. N. Lima, and J. Xie, "Argo data assimilation into HYCOM with an EnOI method in the Atlantic Ocean," *Ocean Sci.*, vol. 11, no. 1, pp. 195–213, 2015, doi: 10.5194/os-11-195-2015.

[47] E. C. Hunke, W. H. Lipscomb, A. K. Turner, N. Jeffery, and S. Elliott, "CICE : The Los Alamos sea ice model documentation and software user's manual version 5.1 LA-CC-06-012," *T-3 Fluid Dyn. Group Los Alamos Nat. Lab.*, vol. 675, pp. 1–115, 2015.

[48] G. Danabasoglu et al., "The community Earth system model version 2 (CESM2)," *J. Adv. Model. Earth Syst.*, vol. 12, no. 2, 2020, Art. no. e2019MS001916, doi: 10.1029/2019MS001916.

[49] A. K. Turner, E. C. Hunke, and C. M. Bitz, "Two modes of sea-ice gravity drainage: A parameterization for large-scale modeling," *J. Geophys. Res. Oceans*, vol. 118, no. 5, pp. 2279–2294, 2013, doi: 10.1002/jgrc.20171.

[50] A. V. Wilchinsky and D. L. Feltham, "Modelling the rheology of sea ice as a collection of diamond-shaped floes," *J. Non-Newtonian Fluid Mech.*, vol. 138, no. 1, pp. 22–32, 2006, doi: 10.1016/j.jnnfm.2006.05.001.

[51] E. C. Hunke, D. A. Hebert, and O. Lecomte, "Level-ice melt ponds in the Los Alamos sea ice model, CICE," *Ocean Model.*, vol. 71, pp. 26–42, Nov. 2013, doi: 10.1016/j.ocemod.2012.11.008.
[52] W. H. Lipscomb, E. C. Hunke, W. Maslowski, and J. Jakacki, "Ridging, strength, and stability in high-resolution sea ice models," *J. Geophys. Res. Oceans*, vol. 112, no. 3, Mar. 2007, Art. no. C03S91, doi: 10.1029/2005JC003355.
[53] M. Kanamitsu et al., "NCEP–DOE AMIP-II reanalysis (R-2)," *Bull. Amer. Meteorol. Soc.*, vol. 83, no. 11, pp. 1631–1644, Nov. 2002, doi: 10.1175/BAMS-83-11-1631.
[54] R. W. Reynolds, T. M. Smith, C. Liu, D. B. Chelton, K. S. Casey, and M. G. Schlax, "Daily high-resolution-blended analyses for sea surface temperature," *J. Climate*, vol. 20, no. 22, pp. 5473–5496, Nov. 2007, doi: 10.1175/2007JCLI1824.1.
[55] R. Wedd et al., "ACCESS-S2: The upgraded bureau of meteorology multi-week to seasonal prediction system," *J. Southern Hemisphere Earth Syst. Sci.*, vol. 72, no. 3, pp. 218–242, Dec. 2022, doi: 10.1071/es22026.
[56] F. S. Castruccio et al., "An EnOI-based data assimilation system with DART for a high-resolution version of the CESM2 ocean component," *J. Adv. Model Earth Syst.*, vol. 12, no. 11, Nov. 2020, Art. no. e2020MS002176, doi: 10.1029/2020MS002176.
[57] J. Lee, Y. Ham, J. Kim, and P. Chang, "Generation of state-dependent ensemble perturbations based on time-varying seawater density for GloSea5 initialization," *Quart. J. Roy. Meteorol. Soc.*, vol. 31, Aug. 2024, Art. no. 29862, doi: 10.1002/qj.4833.
[58] P. R. Oke, P. Sakov, and S. P. Corney, "Impacts of localisation in the EnKF and EnOI: Experiments with a small model," *Ocean Dyn.*, vol. 57, no. 1, pp. 32–45, 2007, doi: 10.1007/s10236-006-0088-8.
[59] Z. Toth and E. Kalnay, "Ensemble forecasting at NCEP and the breeding method," *Monthly Weather Rev.*, vol. 125, no. 12, pp. 3297–3319, 1997, doi: 10.1175/1520-0493(1997)125<3297:EFANAT>2.0.CO;2.
[60] J. Stroeve et al., "A Lagrangian snow evolution system for sea ice applications (SnowModel-LG): Part II—Analyses," *J. Geophys. Res. Oceans*, vol. 125, no. 10, Oct. 2020, Art. no. e2019JC015913, doi: 10.1029/2019JC015900.
[61] G. E. Liston et al., "A Lagrangian snow-evolution system for sea-ice applications (SnowModel-LG): Part I—Model description," *J. Geophys. Res. Oceans*, vol. 125, no. 10, Oct. 2020, Art. no. e2019JC015913, doi: 10.1029/2019JC015913.
[62] J. Zhang and D. A. Rothrock, "Modeling global sea ice with a thickness and enthalpy distribution model in generalized curvilinear coordinates," *Monthly Weather Rev.*, vol. 131, no. 5, pp. 845–861, 2003, doi: 10.1175/1520-0493(2003)131<0845:MGSIWA>2.0.CO;2.
[63] R. Ricker, S. Hendricks, L. Kaleschke, X. Tian-Kunze, J. King, and C. Haas, "A weekly Arctic sea-ice thickness data record from merged CryoSat-2 and SMOS satellite data," *Cryosphere*, vol. 11, pp. 1607–1623, 2017, doi: 10.5194/tc-2017-4.
[64] H. Melling, P. H. Johnston, and D. A. Riedel, "Measurements of the underside topography of sea ice by moored subsea sonar," *J. Atmos. Ocean Technol.*, vol. 12, no. 3, pp. 589–602, Jun. 1995, doi: 10.1175/1520-0426(1995)012<0589:MOTUTO>2.0.CO;2.
[65] C. J. Planck, J. Whitlock, C. Polashenski, and D. Perovich, "The evolution of the seasonal ice mass balance buoy," *Cold Regions Sci. Technol.*, vol. 165, Sep. 2019, Art. no. 102792, doi: 10.1016/j.coldregions.2019.102792.
[66] K. C. Jezek et al., "Remote sensing of sea ice thickness and salinity with 0.5-2 GHz microwave radiometry," *IEEE Trans. Geosci. Remote Sens.*, vol. 57, no. 11, pp. 8672–8684, Nov. 2019, doi: 10.1109/TGRS.2019.2922163.
[67] G. A. Maykut, "The surface heat and mass balance," in *The Geophysics of Sea Ice*. Boston, MA, USA: Springer, 1986, pp. 395–463, doi: 10.1007/978-1-4899-5352-0_6.
[68] G. A. Maykut and D. K. Perovich, "The role of shortwave radiation in the summer decay of a sea ice cover," *J. Geophys. Res. Oceans*, vol. 92, no. C7, pp. 7032–7044, Jun. 1987, doi: 10.1029/JC092iC07p07032.
[69] F. Massonnet, M. Vancoppenolle, H. Goosse, D. Docquier, T. Fichefet, and E. Blanchard-Wrigglesworth, "Arctic sea-ice change tied to its mean state through thermodynamic processes," *Nature Climate Change*, vol. 8, no. 7, pp. 599–603, 2018, doi: 10.1038/s41558-018-0204-z.
[70] M. C. Serreze and A. P. Barrett, "Characteristics of the Beaufort sea high," *J. Climate*, vol. 24, no. 1, pp. 159–182, Jan. 2011, doi: 10.1175/2010JCLI3636.1.
[71] R. Song, L. Mu, S. N. Loza, F. Kauker, and X. Chen, "Improves Arctic sea-ice forecast," *Geophys. Res. Lett.*, vol. 51, 2024, Art. no. e2024GL110405, doi: 10.22541/essoar.170680251.16100147/v1.
[72] H. Shi et al., "Estimation of Arctic winter snow depth, sea ice thickness and bulk density, and ice freeboard by combining CryoSat-2, AVHRR, and AMSR measurements," *IEEE Trans. Geosci. Remote Sens.*, vol. 61, Apr. 2023, Art. no. 4300718, doi: 10.1109/TGRS.2023.3265274.
[73] J.-M. Kim et al., "The estimation of the total freeboard of Arctic sea ice in winter using passive microwave satellite measurements," *J. Atmos. Ocean Technol.*, vol. 39, no. 10, pp. 1611–1627, Oct. 2022, doi: 10.1175/jtech-d-21-0105.1.

Jeong-Gil Lee received the B.S. degree in earth and environmental sciences from Chonnam National University, Gwangju, South Korea, in 2015, and the M.S. and Ph.D. degrees in oceanography, Chonnam National University, Gwangju, South Korea, in 2017 and 2023, respectively.

From 2023 to 2024, he was a Postdoctoral Research Scientist with the Center for Sustainable Environment Research, Korea Institute of Science and Technology. He is currently a Postdoctoral Research Scientist with Environmental Planning Institute, Seoul National University, Seoul, South Korea. His research interests include ensemble-based data assimilation for satellite-derived sea ice data and in situ oceanic observation data.

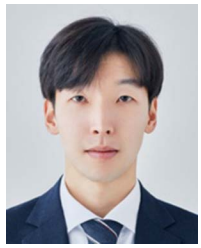

Daehyun Kang received the B.S. degree in earth science and engineering, and environmental analysis and pollution control engineering and the Ph.D. degree in environmental science and engineering from the Ulsan National Institute of Science and Technology, Ulsan, South Korea, in 2012 and 2019, respectively.

From 2019 to 2021, he was a Postdoctoral Research Scientist with the Department of Atmospheric Sciences, University of Washington, Seattle, USA. From 2021 to 2022, he was a Research Professor with Chonnam National University. He is currently a Senior Researcher with the Center for Climate and Carbon Cycle Research, Korea Institute of Science and Technology, Seoul, South Korea. His research interests include subseasonal ensemble forecast via deep learning and deep-learning-based estimation and prediction of precipitation and air quality.

Joo-Hong Kim received the B.S. degree in atmospheric sciences and the Ph.D. degree in earth and environmental sciences from Seoul National University, Seoul, South Korea, in 2000 and 2005, respectively.

From 2005 to 2007, he was a Postdoctoral Research Scientist with the Research Institute of Basic Sciences, Seoul National University. From 2007 to 2008, he was a Postdoctoral Research Scientist with Brain Korea 21 Plus Project. From 2008 to 2010, he was a Researcher with Met Office Hadley Centre, U.K. From 2010 to 2012, he was an invited Research Professor of atmospheric sciences with National Taiwan University. He is currently working as a Senior Researcher with Korea Polar Research Institute, Incheon, South Korea. His research interests include the coupled physical processes controlling the sea ice variability, the mechanisms of polar climate change, and the pole-to-midlatitude weather/climate linkages.

Jong-Min Kim received the B.S. and Ph.D. degrees in earth and environmental sciences from Seoul National University, Seoul, South Korea, in 2015 and 2023, respectively.

He is currently working as a Postdoctoral Researcher with Korea Polar Research Institute, Incheon, South Korea. His research interests include sea ice thickness retrieval and relevant sea ice parameters using passive microwave satellite.

Sang-Moo Lee (Member, IEEE) received the B.S. and Ph.D. degrees in earth and environmental sciences from Seoul National University, Seoul, South Korea, in 2011 and 2018, respectively.

From 2018 to 2019, he was a Postdoctoral Research Scientist with Satellite Meteorology Laboratory, Seoul National University, where he was an Assistant Research Professor of Brain Korea 21 Plus Project in 2019. From 2019 to 2022, he was a Postdoctoral Research Fellow with the Center for Environmental Technology, Department of Electrical, Computer, and Energy Engineering, University of Colorado Boulder, Boulder, CO, USA, where he was a Visiting Scholar with the National Snow and Ice Data Center, Cooperative Institute for Research in Environmental Sciences. He is currently an Assistant Professor with the School of Earth and Environmental Sciences, Seoul National University. His research interests include satellite remote sensing, the utilization of satellite measurements for the study of oceanic and atmospheric processes, and the modeling of the atmospheric radiative transfer and surface emissivity.

Yoo-Geun Ham received the B.S. and Ph.D. degrees in earth and environmental sciences from Seoul National University, Seoul, South Korea, in 2003 and 2009, respectively.

From 2009 to 2010, he was a Postdoctoral Researcher with Basic Science Research Institute, Seoul National University. He was a Scientist 1 from 2010 to 2012 and a Scientist 2 from 2012 to 2013 with Global Modeling and Assimilation Office, NASA Goddard Space Flight Center. He was an Assistant Professor from 2013 to 2016, an Associate Professor from 2016 to 2021, and a Professor from 2021 to 2024 with the Department of Oceanography, Chonnam National University. He is currently an Associate Professor with the Department of Environmental Managements, Graduated School of Environmental Studies, Seoul National University. His research interests include AI-based climate modeling/prediction, climate change detection, data assimilation, and carbon cycle prediction, ensemble-based oceanic/sea-ice data assimilation, statistical postprocessing, and climate variability/climate change mechanism.